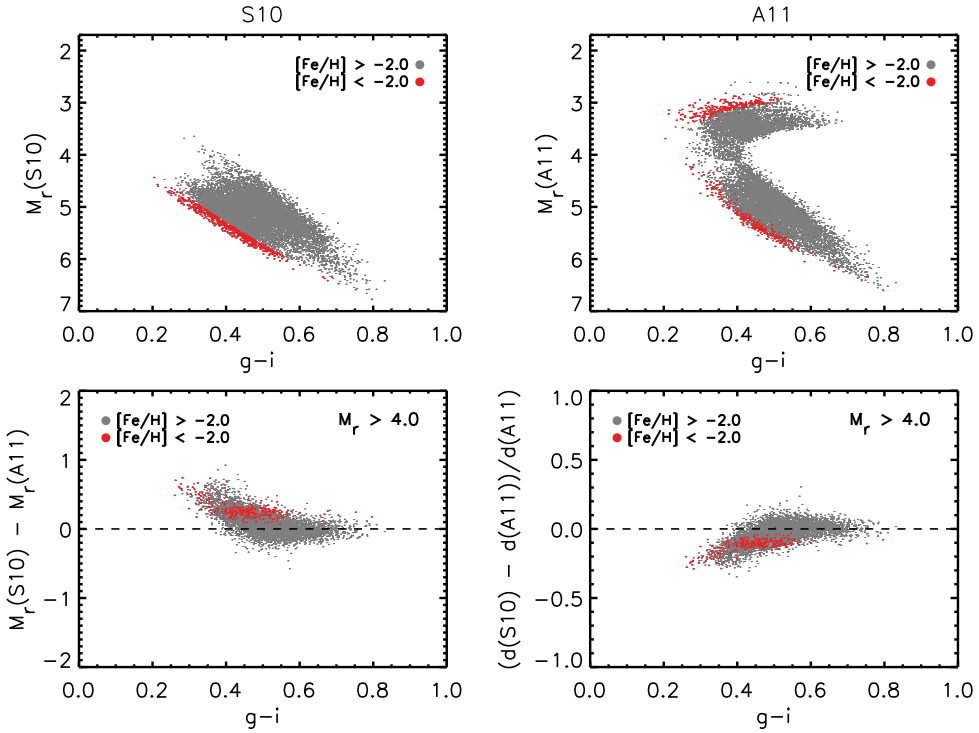

Figure 5. Upper left: M_r, $g-i$ CMD for stars with spectroscopically assigned D classifications, with absolute magnitudes calculated from Equation (A1) of I08, as adopted by S10. Upper right: M_r, $g-i$ CMD for stars with spectroscopically assigned D classifications, with absolute magnitudes calculated using the calibrated isochrone fitting procedures of A12. The stars with [Fe/H] > -2.0 are shown as gray dots, while those with [Fe/H] < -2.0 are shown as red dots. Lower left: difference between the M_r absolute magnitudes for stars with spectroscopically assigned D classifications for the S10 and A12 calculations, as a function of $g-i$. Lower right: fractional change in derived distances from those adopted by S10 as compared to those adopted by A12, as a function of $g-i$.

3.2. The Calibrated Isochrone Approach

Distances to individual stars can also be estimated using a set of stellar isochrones, once they have been properly calibrated against the observed colors and magnitudes of stars with known distances and ages. For the present exercise, we follow the prescription in An et al. (2009a) to derive distances to individual stars employing stellar isochrones with empirical corrections on the colors (An et al. 2009b). This calibration was based on photometry from An et al. (2008) for a number of open and globular clusters, including M67 ([Fe/H] $= 0.0$) and M92 ([Fe/H] $= -2.4$), which provides metallicity-dependent color corrections in $ugriz$ over the metallicity range under consideration. A full description of the isochrone calibration can be found in A12.

After correcting the photometry for dust extinction, we performed model fits over the full parameter space (with metallicity range $-3.0 \leqslant$ [Fe/H] $\leqslant +0.4$). We included $griz$ photometry and the key SSPP atmospheric parameters ([Fe/H], $\log g$, $T_{\rm eff}$) in the model fits, and found a best-fitting model by searching for a minimum χ^2 of the fit. Note that, for consistency with the other approaches, the corrected metallicity [Fe/H]$_C$ was employed. We assumed minimum errors in the photometry of 0.01 mag for gri and 0.02 mag for z, and took conservative errors of 0.3 dex for [Fe/H], 160 K for $T_{\rm eff}$, and 0.4 dex for $\log g$, as characteristic errors in each of these parameters (including possible systematic scale differences between the SSPP and the models). The lower limit of [Fe/H] in the models is -3.0, so we assumed [Fe/H] $= -3.0$ for any stars with metallicity less than this value. This choice has a negligible impact on distance estimation, since the isochrones are insensitive to a change in the atmospheric abundances for [Fe/H] < -3.0. An age of 12 Gyr is assumed for [Fe/H] < -1.0, while 4 Gyr is taken for [Fe/H] > -0.3, with a linearly interpolated value for metallicities between the two boundaries. Solutions for distances were dropped from further consideration in cases where either the fitting process did not converge, or if the final reduced χ^2 of a converged fit exceeded 1.2.

Unlike the original approach described by An et al. (2009a), the calibrated isochrones actually reach into the MSTO region, thus distance estimates are available for both TO and SG stars, in addition to D stars, albeit with lower accuracy in the distance estimates. For the purpose of our present comparisons we only accepted stars with spectroscopic assignments of surface gravity $\log g \geqslant 4.0$. An inter-comparison of results from various color indices indicates that the internal error in the distance modulus is $\sim$0.1 mag; an additional $\sim$0.1 mag error is expected from the errors in age, [Fe/H], [α/Fe], and adopted $E(B-V)$. This suggests that the associated distance-modulus error is $\sim$0.1–0.2 mag for individual stars. As was the case for the I08 approach, the effects of binarity are more difficult to quantify, and are not included in this error estimate (see An et al. 2007).

The upper left panel of Figure 5 shows the CMD obtained using the absolute magnitudes from Equation (A1) of I08 as adopted by S10. The upper right panel shows the CMD for stars with spectroscopic assignments as D ($\log g \geqslant 4.0$), with absolute magnitudes assigned by the calibrated isochrone procedure of A12. Note that in the evaluation of both relationships above, the [Fe/H]$_C$ used by C10 was employed, although similar results are obtained when either the photometric metallicity estimates or the adopted metallicity from the SSPP ([Fe/H]$_A$) were used. The stars are color-coded to indicate metallicities above and below [Fe/H] $= -2.0$. As is clear from inspection of the upper right panel, the A12 procedure assigns roughly

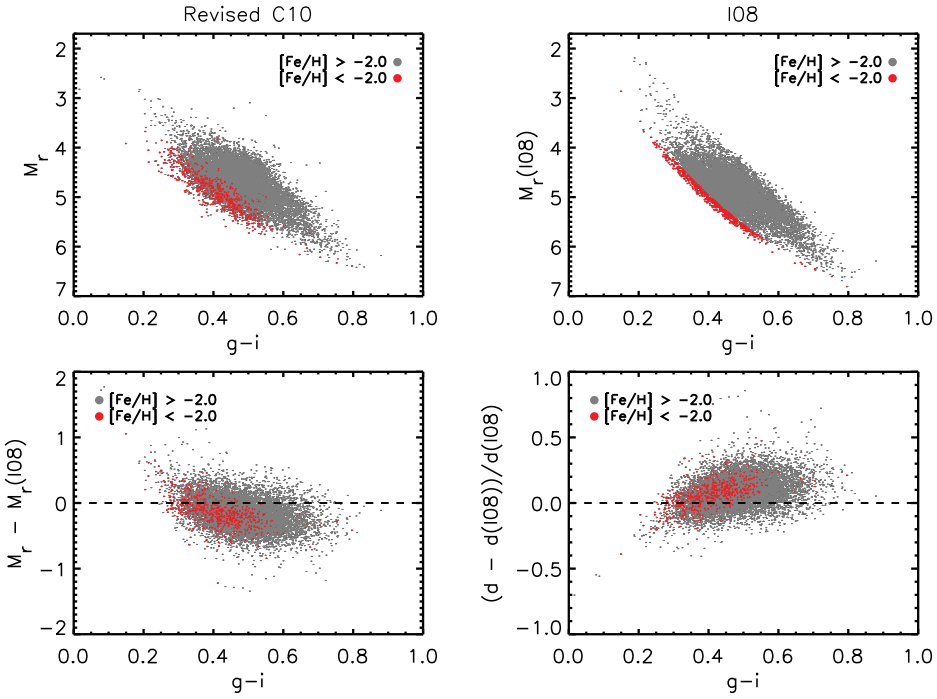

Figure 6. Upper left: M_r, $g-i$ CMD for stars with revised C10 luminosity classifications and with spectroscopically assigned D classifications, as a function of $g-i$. Upper right: M_r, $g-i$ CMD for stars with spectroscopically assigned D classifications, with absolute magnitudes calculated from Equation (A7) of I08, as adopted by I08. The stars with [Fe/H] > -2.0 are shown as gray dots, while those with [Fe/H] < -2.0 are shown as red dots. Lower left: difference between the M_r absolute magnitudes for stars with spectroscopically assigned D classifications for the A12 and I08 calculations, as a function of $g-i$. Lower right: fractional change in the revised distances from C10 as compared to those adopted by I08, as a function of $g-i$.

half of the spectroscopic D stars into SG/G classifications, with correspondingly brighter absolute magnitudes near $M_r \sim 3$.

The lower left panel of Figure 5 shows the difference in the assigned M_r absolute magnitudes that arises when one compares the adopted S10 and A12 relationships for stars spectroscopically classified as D stars. For the purpose of this exercise, we focus on the stars to which the A12 procedure assigns dwarf status, with absolute magnitudes $M_r > 4.0$. For stars with [Fe/H] > -2.0, the S10 determinations are fainter than those of A12 by a median offset of 0.10 mag (rms 0.09 mag) for $0.4 < g-i < 0.8$, while they are fainter by up to 0.7 mag (median offset of 0.31 mag, rms 0.15 mag) for the bluer stars with $g-i < 0.4$. The offsets are significantly larger for stars with [Fe/H] < -2.0. For the redder stars with $0.4 < g-i < 0.8$, the median offset of the S10 determinations compared with A12 is 0.24 mag (rms 0.06 mag) fainter; for bluer stars with $g-i < 0.4$, the median offset is 0.41 mag (rms 0.15 mag) fainter.

The lower right panel of this figure shows the fractional difference in the derived distances between S10 and A12 scales. For stars with [Fe/H] > -2.0 and $0.4 < g-i < 0.8$, the median offset of the S10 distances with respect to the A12 distances is only about 4% (rms 4%). In the bluer range, $g-i < 0.4$, the median offset increases to about 13% (rms 6%). For stars with [Fe/H] < -2.0 and $0.4 < g-i < 0.8$, the median offset of the S10 distances with respect to the A12 distances increases to 10% (rms 3%). In the bluer range, $g-i < 0.4$, the median offset increases to about 17% (rms 6%). All distance differences are in the sense that the S10 scale is shorter than the A12 scale.

3.3. Comparison with the C10 Dwarfs

We now compare the C10 sample, with revised TO classifications, with the calculations of I08 (Figure 6) and with those of A12 (Figure 7). As can be appreciated by inspection of these figures, the absolute magnitude scale for the revised C10 sample agrees well with those from both I08 and A12 (in the latter case, one can only consider the stars considered dwarfs by the A12 procedure; see below).

The lower left panel of Figure 6 shows the difference in the assigned M_r absolute magnitudes that arises when one compares the revised C10 estimates with those of I08 for stars spectroscopically classified as D stars. For stars with [Fe/H] > -2.0, the revised C10 determinations are brighter by a median offset of 0.21 mag (rms 0.16 mag) for $0.4 < g-i < 0.8$, while the median offset of revised C10 absolute magnitudes is 0.14 mag (rms 0.27 mag) brighter for bluer stars in the range $g-i < 0.4$. The offsets are of similar size for stars with [Fe/H] < -2.0. For the redder stars with $0.4 < g-i < 0.8$, the median offset of the revised C10 determinations compared with I08 is 0.23 mag (rms 0.15 mag) brighter; for bluer stars, the median offset is 0.13 mag (rms 0.14 mag) brighter.

The lower right panel of this figure shows the fractional difference in the derived distances between the revised C10 and I08 scales. For stars with [Fe/H] > -2.0 and $0.4 < g-i < 0.8$, the median offset of the revised C10 distances with respect to the I08 distances is 10% (rms 9%). In the bluer range, $g-i < 0.4$, the median offset is about 6% (rms 7%). For stars with [Fe/H] < -2.0 and $0.4 < g-i < 0.8$, the median offset of the revised C10 distances with respect to the I08 distances is 11% (rms 8%). In the bluer range, $g-i < 0.4$, the median offset is 6% (rms 6%). All distance differences are in the sense that the revised C10 scale is longer than the I08 scale.

Turning to Figure 7, if we focus on the stars that are assigned dwarf status by the A12 procedure (we accomplish this by only comparing stars with derived $M_r > 4.0$), the agreement between the revised C10 estimates of absolute magnitude and distance

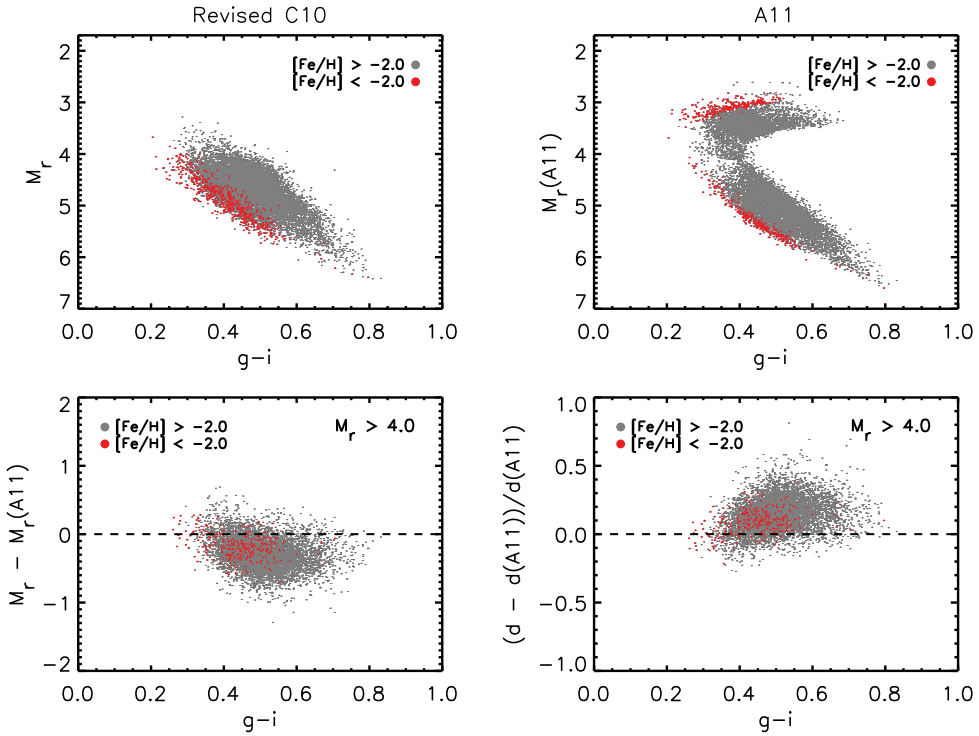

Figure 7. Upper left: M_r, $g-i$ CMD for stars with revised C10 luminosity classifications and with spectroscopically assigned D classifications, as a function of $g-i$. Upper right: M_r, $g-i$ CMD for stars with spectroscopically assigned D classifications, with absolute magnitudes calculated from Equation (A7) of I08, as adopted by I08. The stars with [Fe/H] > -2.0 are shown as gray dots, while those with [Fe/H] < -2.0 are shown as red dots. Lower left: difference between the M_r absolute magnitudes for stars with spectroscopically assigned D classifications for the revised C10 and A12 calculations, as a function of $g-i$. Lower right: fractional change in the revised distances from C10 as compared to those adopted by A12, as a function of $g-i$.

is only slightly worse, with respect to A12, than with respect to I08.

The lower left panel of Figure 7 shows the difference in the assigned M_r absolute magnitudes that arises when one compares the revised C10 estimates with those of A12, for stars spectroscopically classified as D. For stars with [Fe/H] > -2.0, the revised C10 determinations are brighter by a median offset of 0.31 mag (rms 0.18 mag) for $0.4 < g-i < 0.8$, while the median offset of revised C10 absolute magnitudes is 0.17 mag (rms 0.15 mag) brighter for bluer stars in the range $g-i < 0.4$. The offsets are smaller for stars with [Fe/H] < -2.0. For the redder stars with $0.4 < g-i < 0.8$, the median offset of the revised C10 determinations compared with I08 is 0.21 mag (rms 0.14 mag) brighter; for bluer stars with $g-i < 0.4$, the median offset is 0.15 mag (rms 0.12 mag) brighter.

The lower right panel of this figure shows the fractional difference in the derived distances between the revised C10 and A12 scales. For stars with [Fe/H] > -2.0 and $0.4 < g-i < 0.8$, the median offset of the revised C10 distances with respect to the A12 distances is 15% (rms 10%). In the bluer range, $g-i < 0.4$, the median offset decreases to about 8% (rms 8%). For stars with [Fe/H] < -2.0 and $0.4 < g-i < 0.8$, the median offset of the revised C10 distances with respect to the I08 distances is 10% (rms 7%). In the bluer range, $g-i < 0.4$, the median offset is 7% (rms 6%). All distance differences are in the sense that the revised C10 scale is longer than the A12 scale.

3.4. Comparison Between A12 and I08

For completeness, Figure 8 shows the comparison between the isochrone-fitting procedure of A12 and the calculations of I08.

The lower left panel of Figure 8 shows the difference in the assigned M_r absolute magnitudes between the A12 and I08 estimates, for stars spectroscopically classified as D (and with $M_r > 4.0$, in order to only compare the stars considered as dwarfs by the A12 procedure). For stars with [Fe/H] > -2.0, the A12 determinations are fainter by a median offset of 0.10 mag (rms 0.08 mag) for $0.4 < g-i < 0.8$, while the median offset is 0.12 mag (rms 0.08 mag) fainter for bluer stars in the range $g-i < 0.4$. The offsets are smaller for stars with [Fe/H] < -2.0. For the redder stars with $0.4 < g-i < 0.8$, the median offset of the A12 determinations compared with I08 is 0.06 mag (rms 0.06 mag) brighter; for bluer stars with $g-i < 0.4$, the median offset is 0.10 mag (rms 0.08 mag) fainter.

The lower right panel of this figure shows the fractional difference in the derived distances between the A12 and I08 calculations. For stars with [Fe/H] > -2.0 and $0.4 < g-i < 0.8$, the median offset of the A12 distances with respect to the I08 distances is 5% (rms 4%). In the bluer range, $g-i < 0.4$, the offset is also about 5% (rms 4%). For stars with [Fe/H] < -2.0 and $0.4 < g-i < 0.8$, the median offset of the A12 distances with respect to the I08 distances is 3% (rms 3%). In the bluer range, $g-i < 0.4$, the offset is similar, about 4% (rms 4%). The distance differences are in the sense that, for the redder stars, the A12 scale is longer than that of I08, while for the bluer stars, the A12 scale is shorter than that of I08.

If we restrict our attention to the stars with [Fe/H] < -2.0, the ones that matter the most for inferences concerning an outer-halo population, we conclude from the above analysis that the I08 and A12 distance scales are compatible with one another (maximum offsets of around 5%), while the revised C10 distance

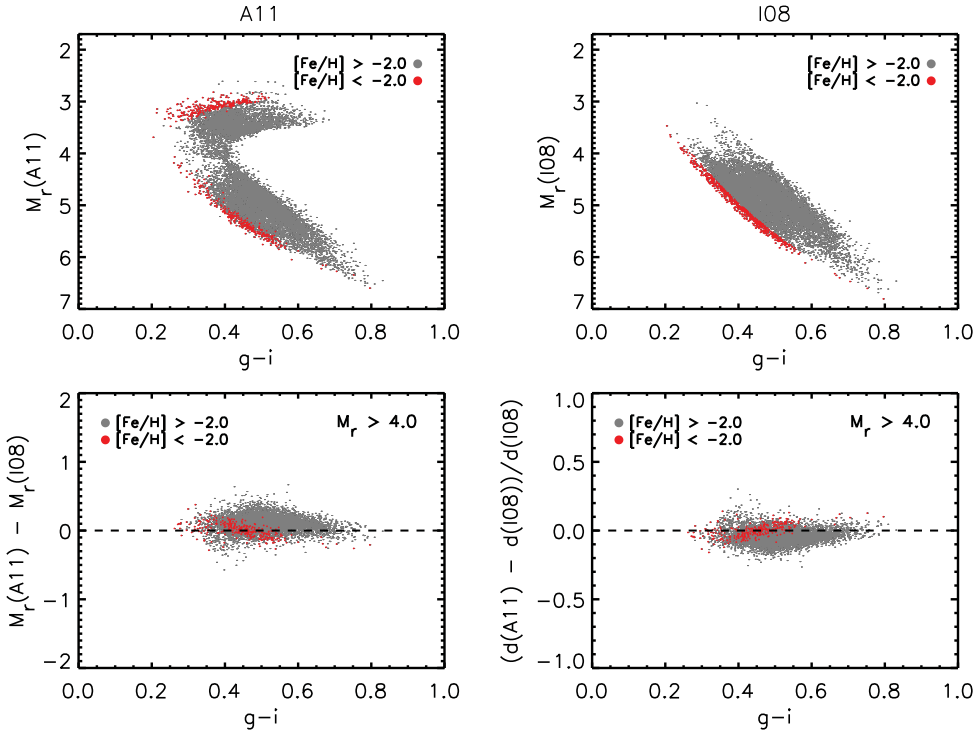

Figure 8. Upper left: M_r, $g - i$ CMD for stars with spectroscopically assigned D classifications, with absolute magnitudes calculated using the calibrated isochrone fitting procedures of A12. Upper right: M_r, $g - i$ CMD for stars with spectroscopically assigned D classifications, with absolute magnitudes calculated from Equation (A7) of I08, as adopted by I08. The stars with [Fe/H] > -2.0 are shown as gray dots, while those with [Fe/H] < -2.0 are shown as red dots. Lower left: difference between the M_r absolute magnitudes for stars with spectroscopically assigned D classifications for the A12 and I08 calculations, as a function of $g - i$. Lower right: fractional change in derived distances from those adopted by A12 as compared to those adopted by I08, as a function of $g - i$.

scale differs (in the sense of being longer) from both the I08 and A12 scales by no more than about 10% (better for stars near the MSTO, around 6%–7%). By contrast, the S10 scale differs (in the sense of being shorter) with respect to the I08 scale by between 10% and 18% (independent of metallicity; worse for stars near the MSTO), and similarly, between 10% and 17% (worse for stars near the MSTO) with respect to the A12 scale. Although it is presently unknown which of these distance scales is closer to "ground truth," the greater disagreement of the S10 scale (in particular close to the MSTO), not only with respect to the revised C10 scale, but also with respect to those of I08 and A12, suggests that it is the S10 scale that should be considered suspect, rather than the revised C10 scale.

4. A REANALYSIS OF KINEMATICS FOR LIKELY OUTER-HALO STARS

We now reconsider a limited kinematic analysis for a local sample of the SDSS DR7 calibration stars following the procedures described by C10, making use of the four different sets of distance assignments discussed above for calculation of the full space motions. In order to provide a fair comparison, we apply the same local volume constraints ($7\,\mathrm{kpc} < R < 10$ kpc and $d < 4$ kpc) to the various samples, but use the values of R and d that would be obtained for each of the different distance scales. This has the obvious result that different numbers of stars will enter into each sample. In order to maximize the contribution from proposed outer-halo stars, we choose to only include stars with [Fe/H] $\leqslant -2.0$. Our purpose is to test the robustness of the retrograde signature that was criticized by S10, which is most evident at low metallicity.

Figure 9 shows histograms of V_ϕ for the stars spectroscopically classified as type D in the revised C10 sample, for all ranges of $Z_{\max}$ (the maximum value of the distance above or below the Galactic plane reached by a given star during its orbit). The red lines shown in each panel are the two components of a model obtained by the R-Mix procedure[16] employed by C10, to which the interested reader is referred for additional details. As can be appreciated from inspection of this figure, all four of the distance calibrations we consider lead to distributions of V_ϕ that include asymmetric tails, which would not be expected to arise for a single-component halo. Naturally, the suggested components and significance of the splits vary from sample to sample; Table 2 summarizes these results. Column 1 lists the sample under consideration (recall that the samples differ only in their adopted distances as described above). Columns 2 and 3 list the inferred means and dispersions (and their errors) of an assumed Gaussian population for the first component of a two-component fit to the observed distribution of V_ϕ, based on the R-Mix procedure. Columns 4 and 5 list the same quantities for the second component (where required). Column 6 is the p-value of the fits to a one-component model.

The first section of Table 2 concerns the parameters of the R-Mix fits, for D stars only, associated with Figure 9, which applies to stars at all $Z_{\max}$. Note that the number of dwarfs listed in the revised C10 sample is more than twice that in the other samples; this is the result of the inclusion of the reclassified TO $\rightarrow$ D described above (including a subset of the stars with $3.75 \leqslant \log g < 4.00$). In the other samples, only the stars with spectroscopic estimates $\log g \geqslant 4.0$ are

[16] http://www.math.mcmaster.ca/peter/mix/mix.html

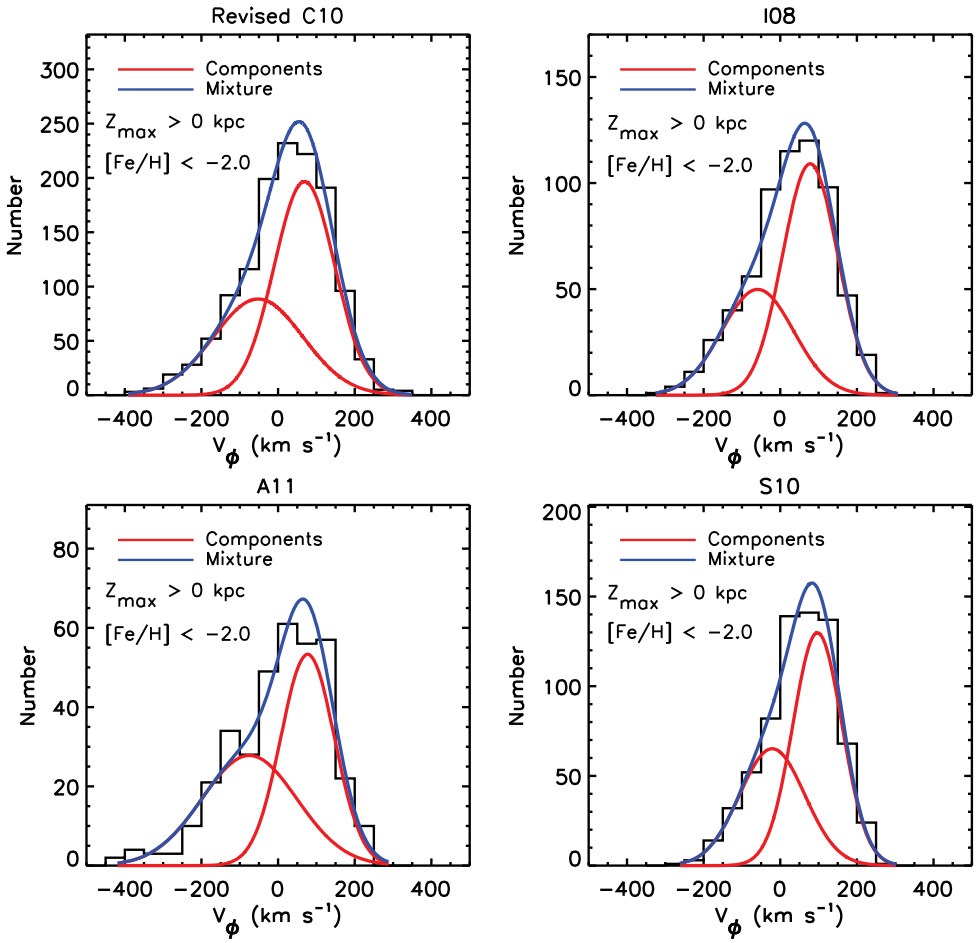

Figure 9. Upper left: histogram of V_ϕ for stars with revised C10 distances, with spectroscopically assigned D classifications, [Fe/H] < -2.0, and all values of Z_{max}. The red solid lines are the suggested components from the R-Mix procedure, while the blue solid line is the final mixture model. Upper right: similar, for D stars with I08 distances. Lower left: similar, for D stars with A12 distances. Lower right: similar, for D stars with S10 distances.

(A color version of this figure is available in the online journal.)

included. From inspection of the table, the suggested splits from R-Mix all include a retrograde and a prograde component, and are highly statistically significant (in the sense that a one-component fit is strongly rejected). This even includes the S10 sample, although one can see that the formal derived velocity for the first component is less retrograde than found for the other samples.

Figure 10 shows the result of a similar analysis for the four different sets of distance calibrations, but restricted to only include stars with derived estimates of $Z_{max} > 5$ kpc. The samples of spectroscopically classified D stars on orbits that reach beyond 5 kpc from the disk plane is much smaller than considered for all ranges of Z_{max}, but the fraction of likely outer-halo stars included by this cut on Z_{max} should be increased.

Inspection of Figure 10 reveals some interesting differences. While the revised C10 sample (which is considerably larger than the other samples) shown in the upper left panel exhibits a clear asymmetric tail extending to negative V_ϕ, the tails of the I08 and A12 samples are weaker than previously, but located at larger negative values of V_ϕ. We judge this to be primarily the result of the smaller numbers of stars included. Of particular interest is the lower right panel, which shows the result for the S10 sample. As can be seen, if one were to accept the S10 absolute magnitude scale and corresponding distances, one would indeed be driven to interpret at least this cut on the data as well represented by a single component, which was the essence of the argument presented by S10.

The second section of Table 2 concerns the parameters of the R-Mix fits, for D stars only, associated with Figure 10. From inspection of the table, the suggested splits from R-Mix include a retrograde and a prograde component for the revised C10 sample, the I08 sample, and the A12 sample, all of which are highly statistically significant, but *not* for the S10 sample, which only allows for a marginally prograde one-component fit. It is revealing that the inferred prograde velocities for the second components have dropped considerably from the case that considered all values of Z_{max}. Of course, it should be kept in mind that the restriction here, for the purpose of comparison using the D stars only, has resulted in rather small numbers of stars included for the I08, A12, and S10 subsamples. For example, the split of the A12 sample to include a highly retrograde, low dispersion, component is presumably driven by small number statistics.

Finally, we consider a similar set of analyses for the full revised C10 sample, including the D, TO, and SG/G classifications and their associated distances and derived space motions. Figure 11 shows the results of this exercise for both the full range of Z_{max} (left panel) and the case where only stars with

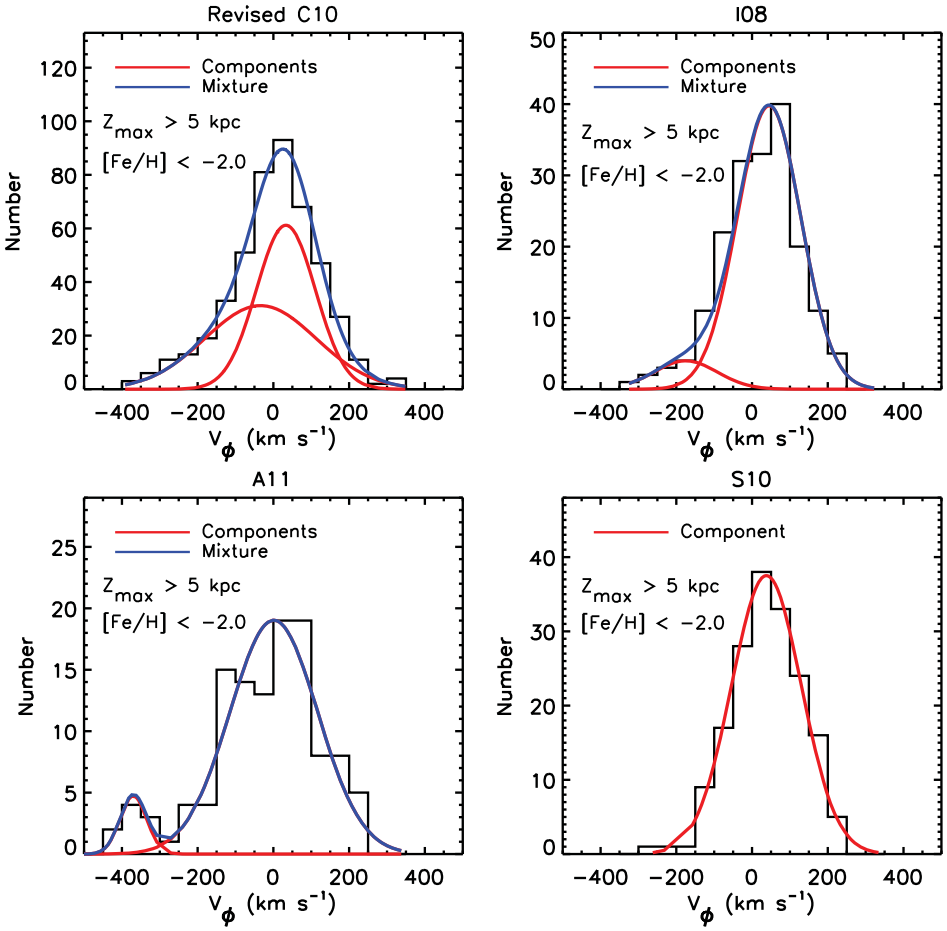

Figure 10. Upper left: histogram of V_ϕ for stars with revised C10 distances, with spectroscopically assigned D classifications, [Fe/H] < -2.0, and $Z_{max} > 5$ kpc. The red solid lines are the suggested components from the R-Mix procedure, while the blue solid line is the final mixture model. Upper right: similar, for D stars with I08 distances. Lower left: similar, for D stars with A12 distances. Lower right: similar, for D stars with S10 distances.

(A color version of this figure is available in the online journal.)

Table 2
R-Mix Results for the Low-metallicity Subsample: Kinematic Parameters

Sample	Number	$\langle V_{\phi,\mathrm{I}}\rangle$ (km s^{-1})	$\sigma_{V_{\phi,\mathrm{I}}}$ (km s^{-1})	$\langle V_{\phi,\mathrm{II}}\rangle$ (km s^{-1})	$\sigma_{V_{\phi,\mathrm{II}}}$ (km s^{-1})	p-value One-component
Spectroscopically Identified Dwarfs						
[Fe/H] < -2.0; $Z_{max} > 0$ kpc						
Rev. C10	1298	-77 ± 57	117 ± 15	44 ± 11	79 ± 10	<0.001
I08	635	-84 ± 66	94 ± 21	53 ± 20	72 ± 8	<0.001
A12	360	-100 ± 28	124 ± 11	52 ± 12	70 ± 8	<0.001
S10	694	-46 ± 47	85 ± 11	72 ± 14	64 ± 8	<0.001
[Fe/H] < -2.0; $Z_{max} > 5$ kpc						
Rev. C10	469	-59 ± 20	147 ± 11	8 ± 10	78 ± 11	<0.001
I08	184	-200 ± 40	83 ± 28	20 ± 8	84 ± 6	<0.001
A12	173	-395 ± 15	35 ± 12	-24 ± 12	116 ± 9	<0.001
S10	119	13 ± 7	92 ± 5	...	...	0.8
All stars—D, TO, and SG/G						
[Fe/H] < -2.0; $Z_{max} > 0$ kpc						
Rev. C10	1471	-91 ± 23	124 ± 8	40 ± 9	80 ± 7	<0.001
[Fe/H] < -2.0; $Z_{max} > 5$ kpc						
Rev. C10	577	-94 ± 23	153 ± 9	12 ± 10	83 ± 10	<0.001

$Z_{max} > 5$ kpc are considered. Inspection reveals the clear presence of an asymmetric tail toward negative V_ϕ in both cases, which we associate with the outer-halo component, as also concluded by C07 and C10.

The last two sections of Table 2 apply to the samples shown in Figure 11. As can be seen from inspection of this table, the mean velocity of the retrograde component is similar to that obtained by C10 for $Z_{max} > 5$ kpc, albeit with a slightly larger formal error

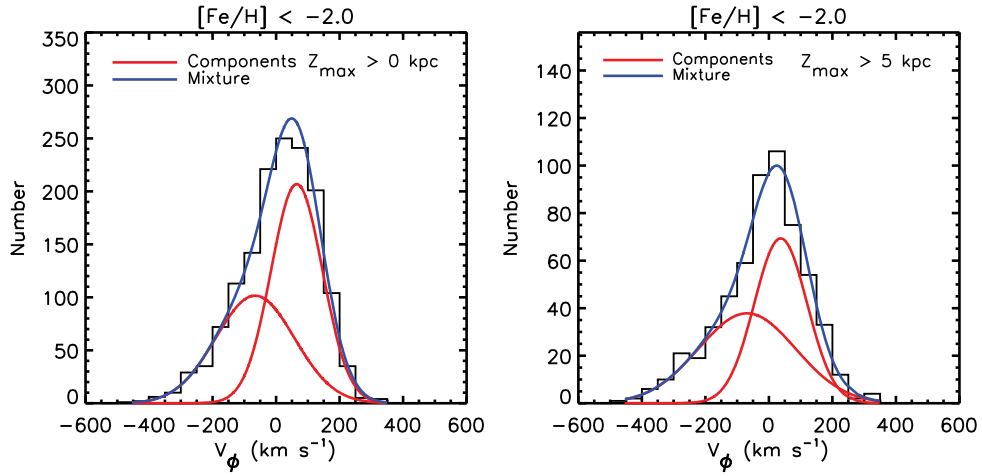

Figure 11. Left panel: histogram of V_ϕ for stars with revised C10 distances, with spectroscopically assigned D, TO, and SG/G classifications, [Fe/H] < -2.0, and all values of $Z_{\rm max}$. The red solid lines are the suggested components from the R-Mix procedure, while the blue solid line is the final mixture model. Right panel: similar, but for stars with $Z_{\rm max} > 5$ kpc.

(A color version of this figure is available in the online journal.)

(-94 ± 23 km s^{-1} versus -80 ± 13 km s^{-1}). The dispersions of the components are also similar to those obtained previously. A one-component halo is strongly rejected in both cases. In all of the above, it should be recalled that the final results given by C10 for the parameters of the various suggested populations were derived with a custom maximum-likelihood procedure, not from the R-Mix procedure described above. Hence, small differences are expected in the final derived values.

Finally, it is worth recalling that Deason et al. (2011) speculated that the retrograde signature they find for a large sample of low-metallicity SDSS blue horizontal-branch (BHB) stars (see further discussion below) could be due to an incorrect adopted value for the local standard of rest (LSR) rotation velocity. However, from inspection of the lower portion of Table 2, one notes that significant *differences* in the mean rotational velocities appear, indicating that a velocity shear is present between the presumed underlying populations, as it is for the Deason et al. (2011) sample as well. Thus, regardless of whether one assigns physical meaning to the presence of a truly retrograde signature associated with the outer-halo component, all indications suggest that there is indeed a difference between the rotational properties of the inner-halo and outer-halo components.

5. ADDITIONAL TESTS FOR THE PRESENCE OF A KINEMATICALLY AND/OR CHEMICALLY DISTINCT OUTER HALO

The limited kinematic analysis carried out above is already strong evidence for the need of more than a single-component halo for the Milky Way, and provides insight as to why a dual-halo interpretation was not supported by S10, when using their adopted absolute magnitude scale. Nevertheless, additional tests of a complex halo model that are not strongly influenced by the adopted distance scale (other than for sample selection) are useful to carry out. In this section, we consider four such pieces of evidence—(1) the origin of the retrograde signature from the revised C10 D classifications as well as for the full set of D, TO, and SG/G classifications, (2) changes in the as-observed MDF of the revised C10 sample (including stars without measured proper motions and located outside the local samples considered in the kinematic analysis), (3) the observed distribution of Galactocentric radial velocities for the well-selected sample of BHB stars from SDSS DR8 discussed by Xue et al. (2011), and (4) changes in the as-observed MDF of the BHB sample over different cuts in Galactocentric distance.

5.1. Additional Evidence (1): The Origin of the Retrograde Signature

It is useful to ask if the single-halo hypothesis, e.g., a halo as described by the best-fit kinematic model from Bond et al. (2010; and argued to be valid by S10), can be rejected even without making use of the analysis of full space motions. The gist of the difficulty with the single-halo hypothesis is the fact that the derived rotational velocity distribution is asymmetric for stars with low [Fe/H] (this asymmetry is already present for stars with [Fe/H] < -1.5, and becomes even stronger for stars with [Fe/H] < -2.0).

The fraction of low-metallicity stars with highly retrograde motions ($V_\phi < -200$ km s^{-1}) in the SDSS/SEGUE DR7 calibration-star sample is significantly larger than for those with highly prograde motions. For stars with [Fe/H] < -1.5 (and exploring $Z_{\rm max} > 0$ kpc), the fraction of stars with highly retrograde motions is 9%, compared with 4% of stars with highly prograde motions ($V_\phi > 200$ km s^{-1}). For stars with [Fe/H] < -2.0, the fractions are 13% highly retrograde compared with 5% highly prograde. For orbits reaching to larger distances from the Galactic plane, $Z_{\rm max} > 5$ kpc, the asymmetry is even stronger (as expected), 16% compared with 5% for [Fe/H] < -1.5, and 20% compared with 6% at [Fe/H] < -2.0. This asymmetric behavior is present even when only spectroscopically classified dwarfs are considered (Figures 9 and 10), which alleviates concerns about potential systematic distance errors associated with the other stellar classifications.

Belief in the reality of the derived asymmetry in the rotation velocities leads naturally to several important questions. For example, "Are stars in the highly retrograde subsample different in any other measured property than the rest of sample?," and "Why do they possess such large inferred retrograde velocities?."

Figure 12 shows that the distributions of the g-band apparent magnitudes and $g - i$ colors are very similar for the full sam-